

# Generalized Mutual Information-Maximizing Quantized Decoding of LDPC Codes

Peng Kang<sup>†</sup>, Kui Cai<sup>†</sup>, Xuan He<sup>†</sup>, Jinhong Yuan<sup>\*</sup>

<sup>†</sup>Singapore University of Technology and Design (SUTD), Singapore, 487372

<sup>\*</sup>The University of New South Wales, Sydney, Australia, 2032

**Abstract**—In this paper, we propose a general framework of the mutual information-maximizing (MIM) quantized decoding for low-density parity-check (LDPC) codes, which can outperform the state-of-the-art lookup table (LUT) decoder by using simple mappings and fixed-point additions for the node updates. Our decoding method is generic in the sense that it can be applied to LDPC codes with arbitrary degree distributions, and it can be implemented based on either the belief propagation (BP) algorithm or the min-sum (MS) algorithm, leading to the MIM quantized BP (MIM-QBP) decoder and the MIM quantized MS (MIM-QMS) decoder, respectively. In particular, we approximate the check node (CN) update of the MIM-QBP decoder by a max-product operation and obtain the MIM-QMS decoder, which simplifies the decoder design and requires less resource consumption. To avoid the precision degradation, we introduce a dynamic reconstruction method to optimize the variable node update for different iterations. Some practical aspects of the proposed decoders such as the design and decoding complexity are also discussed. Simulation results show that the MIM-QBP decoder outperforms the LUT decoders in the waterfall region with both 3-bit and 4-bit precision. Moreover, the 4-bit MIM-QMS decoder can even surpass the floating-point BP decoder in the error-floor region.

**Index Terms**—Low-density parity-check (LDPC) codes, lookup table (LUT), mutual information-maximizing (MIM), quantization.

## I. INTRODUCTION

Low-density parity-check (LDPC) codes [1] and their variations [2]–[7] have been widely applied to wireless communication and data storage systems, for their capacity approaching performance under iterative message passing decoding [8]. Many researchers have put their efforts on the development of the LDPC decoders in terms of the decoding algorithms [9]–[12] and architectures [13]–[17], for achieving a good trade-off between the error performance and decoding complexity. Most of these LDPC decoders make use of the messages represented by log-likelihood ratios (LLRs). For practical systems, LDPC decoders require a finite precision and hence quantization is necessary to be performed on the LLRs, leading to the fixed-point message passing decoding.

In the fixed-point implementation of LDPC decoders, many efforts have been devoted to the quantizer design [18]–[25] to improve the error performance in the waterfall or the error-floor region. In particular, the uniform quantization schemes were proposed in [18]–[20] to increase the precision of quantized messages. However, there is significant performance loss using uniformly quantized messages with low precision (e.g., 5–7 bits). Moreover, as shown in [19], the belief propagation

(BP) decoder [9] with uniform quantization demonstrates a high error floor due to the existence of absorbing sets [26]. To overcome these problems, non-uniform quantization schemes are investigated in [21]–[24], which attract much attention due to their excellent performance with low-precision quantization. For example, the quantized BP decoder in [21] is implemented based on simple mappings and fix-point additions to achieve low decoding complexity. However, the decoder design in [21] requires a large amount of manual optimization to obtain the quantizer parameters, and hence there lacks a systematic way to generalize the design for different LDPC codes.

An alternative approach to realize non-uniform quantization for the LDPC decoders is to adopt lookup tables (LUTs) for the variable node (VN) and the check node (CN) updates. Recently, mutual information-maximizing lookup table (MIM-LUT) decoders were proposed in [27]–[31]. They replace the arithmetic computation for the node updates by table lookup, where the LUTs are designed based on an optimal or a sub-optimal quantizer and the density evolution (DE) [8] to maximize the mutual information between the quantized message and the associated codeword bit. The optimal quantizer in [27] is obtained by using the dynamic programming (DP) [23]. In [28], Lewandowsky et al. utilized the information bottleneck method to generate the LUTs for regular LDPC codes, and proposed the so-called information optimum decoder [32]. Following [28], Stark et al. extended the framework of the information optimum decoder and proposed the message alignment method in [29] for the decoding of irregular LDPC codes. The message alignment method was further improved in [30] by considering the degree distributions of the LDPC codes in the design of the LUTs for nodes with different degrees. The min-LUT decoder was proposed in [31] for the decoding of irregular LDPC codes, which provides a systematic framework for the joint LUTs design based on discrete message passing. In particular, the CN update based on the BP algorithm are replaced by a simpler min update, which is known as the min-sum (MS) algorithm, to reduce the decoding complexity. However, as the size of LUTs grows exponentially with the node degrees, the large LUTs in [27]–[31] have to be decomposed into a series of cascaded small LUTs to reduce the memory usage, where each LUT has binary input and single output symbols. This results in degradation of the decoding error performance due to the loss of mutual information [33].

To avoid the performance loss due to decomposing LUTs, the mutual information-maximizing quantized BP (MIM-QBP) decoder was proposed in [?], [34] for the decoding of regu-

lar LDPC codes. Instead of considering only the two input symbols in the LUT design, the MIM-QBP decoder maps each incoming message to a specific number and computes all possible combinations of the outgoing message. Then an optimal quantizer is designed to generate the threshold sets for the node updates. It is shown in [34] that the MIM-QBP decoder with only 3 bits precision can outperform the floating-point BP decoder at the high signal-to-noise ratio (SNR) region for regular LDPC codes with high code rates. Meanwhile, Wang et al. proposed a decoding method in [35] based on reconstruction-computation-quantization (RCQ). Similar to the MIM-QBP decoder, the RCQ decoder reconstructs each input message into a corresponding LLR value. The outgoing message is then computed based on either the BP [21] or the min-sum (MS) [31] algorithm, and the quantizers for the CN and VN updates are obtained through the hierarchical dynamic quantization (HDQ) scheme, respectively. In this way, the RCQ decoder can mitigate the performance degradation caused by LUT decomposition. Note that the reconstructed LLR values are naturally with floating-point precision and require extra quantization to implement the decoder with the finite precision. In addition, the HDQ scheme is a sub-optimal quantization scheme, which sacrifices the error performance for less computational complexity in the decoder design.

In this paper, we generalize the work in [34] and present a systematic framework of the mutual information-maximizing (MIM) quantized decoding for LDPC codes with arbitrary degree distributions. The proposed decoding method only requires simple mappings and fixed-point additions (including subtractions), and hence facilitates easier hardware implementation. The main contributions of this work are summarized below:

- We generalize the framework of the MIM quantized decoding for the LDPC codes with arbitrary degree distributions. In particular, we adopt the MIM quantization to derive the discrete density evolution (DE) for the MIM-QBP decoder. We also compare the differences between the design of the proposed MIM-QBP decoder and that of the existing variants of the LUT decoder.
- We approximate the CN update of the MIM-QBP decoder by a max-product operation and obtain the MIM quantized MS (MIM-QMS) decoder, which significantly reduces the resource consumption and the computational complexity for decoding. In addition, we introduce a fast computation method for the CN update of the MIM-QMS decoder to further simplify the decoder design.
- We discuss the principle of selecting the proper operating threshold for the MIM quantized decoders. We also propose a dynamic reconstruction method to optimize the VN update of the MIM quantized decoders for different decoding iterations. In this way, the reconstructed values can make a full use of the allocated bit precision without precision degradation.
- We present the hardware architectures for the CN and VN updates of the MIM quantized decoder, respectively. The design and decoding complexity of the MIM quantized decoders are also analyzed.

- We design the MIM-QBP and MIM-QMS decoders with 3-bit and 4-bit precision, respectively. The error performance of the designed decoders is evaluated and compared with that of the different LUT decoder variants. Simulation results show that the MIM-QBP decoder can outperform the state-of-the-art LUT decoder with the same message precision in the waterfall region. Moreover, the 4-bit MIM-QMS decoder can even surpass the floating-point BP decoder in the error-floor region for the IEEE 802.3an standard rate 0.84 LDPC code and the IEEE 802.11n standard rate 1/2 LDPC code.

The rest of this paper is organized as follows. In Section II, we review the basic framework of the MIM-QBP decoder for the decoding of regular LDPC codes. In Section III, we present the generalized framework of the MIM-QBP decoder for any ensemble of the LDPC codes that can be characterized by degree distributions. We also highlights the differences in the design of the proposed MIM-QBP decoder compared to the existing LUT decoders. The design of the MIM-QMS decoder based on the max-product operation is introduced in Section IV. Section V discusses the practical concerns of the MIM quantized decoders, including the choice of the channel parameter, the hardware architectures for the node updates, as well as the design and decoding complexity. We also present a dynamic reconstruction method to optimize the VN update. In Section VI, we evaluate the error performance of the proposed MIM-QBP and MIM-QMS decoders and compare it with that of different LUT decoder variants. Section VII concludes the paper.

## II. PRELIMINARIES

In this section, we briefly review the framework of the MIM-QBP decoder for decoding  $(d_v, d_c)$  LDPC codes [34]. As shown in Fig. 1, the design of the node (both CN and VN) updates for the MIM-QBP decoder is divided into three steps: reconstruction, calculation, and quantization. Let  $\mathcal{L} = \{0, 1, \dots, |\mathcal{L}|-1\}$  be the alphabet of the channel output from a symmetric binary-input discrete memoryless channel (DMC). Define  $\mathcal{R} = \{0, 1, \dots, |\mathcal{R}|-1\}$  and  $\mathcal{S} = \{0, 1, \dots, |\mathcal{S}|-1\}$  as the alphabets of variable-to-check (V2C) and check-to-variable (C2V) message, respectively. In general, we set  $|\mathcal{R}| = |\mathcal{S}| = |\mathcal{L}| = 2^{q_m}$  for all iterations, where  $q_m$  is the precision of the message. Denoted by  $L \in \mathcal{L}$ , the message from the DMC output. Denote the V2C (resp. C2V) message by  $R \in \mathcal{R}$  (resp.  $S \in \mathcal{S}$ ).

1) *Reconstruction*  $\phi(\cdot)$ : Let  $\mathcal{M} = \{0, 1, \dots, |\mathcal{M}|-1\}$  be the alphabet of the  $q_m$  incoming message, where  $|\cdot|$  represents the cardinality of the alphabet. Each realization  $\mu_k \in \mathcal{M}$  ( $k = 1, 2, \dots, |\mathcal{M}|$ ) of the incoming message is mapped to a specific number in the computational domain  $\mathbb{D}$ , where in general  $\mathbb{D}$  is considered as real number ( $\mathbb{R}$ ) or integer number ( $\mathbb{Z}$ ). We denote the reconstruction function (RF)  $\phi(\cdot)$  for the channel output by  $\phi_{ch}$ , and those for the CN and VN updates by  $\phi_c$  and  $\phi_v$ , respectively. For the CN update, we have  $\mathcal{M} = \mathcal{R}$  for incoming message  $R$ , and each realization  $r_k \in \mathcal{R}$  of  $R$  is reconstructed by  $\phi_c : \mathcal{R} \rightarrow \mathbb{D}$ . For the VN update, the alphabets of the incoming message become

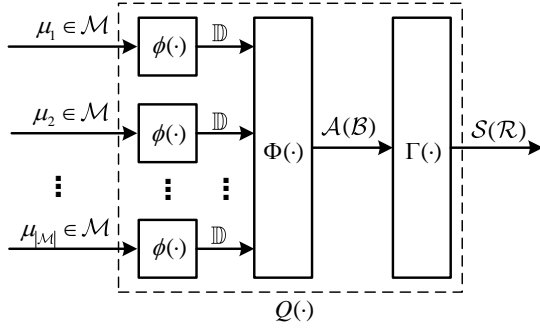


Fig. 1: The framework of the MIM-QBP decoder for decoding the  $(d_v, d_c)$  LDPC codes.

$\mathcal{M} = \mathcal{L}$  for  $L$ , and  $\mathcal{M} = \mathcal{S}$  for  $S$ . A realization  $l \in \mathcal{L}$  of  $L$  is reconstructed by  $\phi_{ch} : \mathcal{L} \rightarrow \mathbb{D}$ , and  $\phi_v$  reconstructs each realization  $s_k \in \mathcal{S}$  of  $S$  as  $\mathcal{S} \rightarrow \mathbb{D}$ .

2) *Calculation*  $\Phi(\cdot)$ : After getting the reconstructed values, a computing function (CF)  $\Phi(\cdot)$  is performed to calculate the alphabet of the outgoing message. We denote the CFs for the CN and the VN updates by  $\Phi_c$  and  $\Phi_v$ , respectively. The maximum number of bits assigned to  $\Phi_c$  and  $\Phi_v$  for representing the outgoing message is set to  $q_c$  and  $q_v$ , respectively. Let  $\mathbf{R} \in \mathcal{R}^{d_c-1}$  be the vector of incoming messages at a CN with degree  $d_c$ . Then  $\mathbf{r} = (r_1, r_2, \dots, r_{d_c-1})$  is a realization of  $\mathbf{R} \in \mathcal{R}^{d_c-1}$ , where  $r_k \in \mathcal{R}$ ,  $k = 1, 2, \dots, d_c - 1$ . In [34],  $\Phi_c$  is implemented based on the BP algorithm as

$$\Phi_c(\mathbf{r}) = \left( \prod_{k=1}^{\dim(\mathbf{r})} \text{sgn}(\phi_c(r_k)) \right) \sum_{k=1}^{\dim(\mathbf{r})} |\phi_c(r_k)|, \quad (1)$$

where  $\dim(\mathbf{r}) = d_c - 1$  is the dimension of  $\mathbf{r}$ , and  $\text{sgn}(\cdot)$  refers to the sign of the message, given by

$$\text{sgn}(\alpha) = \begin{cases} -1, & \alpha < 0, \\ 0, & \alpha = 0, \\ 1, & \alpha > 0. \end{cases}$$

At a VN with degree  $d_v$ , define  $(L, \mathbf{S}) \in \mathcal{L} \times \mathcal{S}^{d_v-1}$  as the vector of incoming messages, where  $\mathbf{S} \in \mathcal{S}^{d_v-1}$  is the vector of incoming messages from the adjacent CNs. Let  $\mathbf{s} = (s_1, s_2, \dots, s_{d_v-1}) \in \mathcal{S}^{d_v-1}$  be a realization of  $\mathbf{S}$ , where  $s_k \in \mathcal{S}$ ,  $k = 1, 2, \dots, d_v - 1$ . Then  $\Phi_v(\cdot)$  combines all the incoming messages as

$$\Phi_v(l, \mathbf{s}) = \phi_{ch}(l) + \sum_{k=1}^{\dim(\mathbf{s})} \phi_v(s_k), \quad (2)$$

where we have  $\dim(\mathbf{s}) = d_v - 1$ . Based on (1) and (2), we can obtain the alphabet of the outgoing message for the CN and the VN updates, respectively. We define the alphabet of the outgoing message computed by  $\Phi_c(\cdot)$  as  $\mathcal{A} = \{a_1, a_2, \dots, a_{|\mathcal{A}|}\} = \{\Phi_c(\mathbf{r}) : \mathbf{r} \in \mathcal{R}^{d_c-1}\}$ , where the elements in  $\mathcal{A}$  are labeled to satisfy  $a_1 \succ a_2 \succ \dots \succ a_{|\mathcal{A}|}$ . Note that  $\succ$  refers to a binary relation on  $\mathbb{R}$  such that  $\alpha \succ \beta \iff (\text{sgn}(\alpha) > \text{sgn}(\beta))$  or  $(\text{sgn}(\alpha) = \text{sgn}(\beta) \text{ and } \alpha < \beta)$  for  $\alpha, \beta \in \mathbb{R}$ . We also denote the alphabet of the outgoing message by  $\mathcal{B} = \{b_1, b_2, \dots, b_{|\mathcal{B}|}\} = \{\Phi_v(l, \mathbf{s}) : (l, \mathbf{s}) \in \mathcal{L} \times \mathcal{S}^{d_v-1}\}$ , where the elements in  $\mathcal{B}$  are labeled to satisfy  $b_1 > b_2 > \dots > b_{|\mathcal{B}|}$ .

3) *Quantization*  $\Gamma(\cdot)$ : In the third step, an optimal sequential deterministic quantizer (SDQ) [36] is adopted to quantize  $q_c$  or  $q_v$  bits outgoing message to  $q_m$  bits extrinsic message. Denoted by  $\Lambda_c = \{\lambda_0 = 0, \lambda_1, \dots, \lambda_{|\mathcal{S}|-1}, \lambda_{|\mathcal{S}|} = |\mathcal{A}|\}$ , the SDQ to quantize  $\mathcal{A} \rightarrow \mathcal{S}$  for the CN update, and denote the SDQ to quantize  $\mathcal{B} \rightarrow \mathcal{R}$  for the VN update by  $\Lambda_v = \{\lambda_0 = 0, \lambda_1, \dots, \lambda_{|\mathcal{R}|-1}, \lambda_{|\mathcal{R}|} = |\mathcal{B}|\}$ . Assume that the channel input  $X$  takes values from  $\mathcal{X} = \{0, 1\}$ . Define the probability mass function (pmf) of  $R$  (resp.  $S$ ) conditioned on the channel input bit  $X$  as  $P_{R|X}$  (resp.  $P_{S|X}$ ). By using the general DP method in [36] and tracking the evolution of  $P_{R|X}$  and  $P_{S|X}$  based on the discrete DE [34], a threshold set (TS) of the SDQ can be determined. We denote the TSs for the CN and the VN updates by  $\Gamma_c$  and  $\Gamma_v$ , respectively.<sup>1</sup> More specifically,  $\Gamma_c$  is given by

$$\Gamma_c = \{\gamma_k : 1 \leq k < |\mathcal{S}|, \gamma_k = a_{\lambda_k}\}, \quad (3)$$

and  $\Gamma_v$  is

$$\Gamma_v = \{\gamma_k : 1 \leq k < |\mathcal{R}|, \gamma_k = b_{\lambda_k}\}. \quad (4)$$

Note that the precision of the MIM-QBP decoder can be fully determined by the parameters  $q_m$ ,  $q_c$ , and  $q_v$ .

We further define the mappings of  $Q_c : \mathcal{R}^{d_c-1} \rightarrow \mathcal{S}$  and  $Q_v : \mathcal{L} \times \mathcal{S}^{d_v-1} \rightarrow \mathcal{R}$ , which consist of the above three steps for designing the CN and the VN updates, respectively. Based on (1) and (3),  $Q_c$  can be represented as

$$Q_c(\mathbf{r}) = \begin{cases} 0, & \Phi_c(\mathbf{r}) \succeq \gamma_1, \\ |\mathcal{S}| - 1, & \gamma_{|\mathcal{S}|-1} \succ \Phi_c(\mathbf{r}), \\ k, & \gamma_k \succ \Phi_c(\mathbf{r}) \succeq \gamma_{k+1}, 1 \leq k \leq |\mathcal{S}| - 2, \end{cases} \quad (5)$$

where  $\succeq$  is defined as a binary relation on  $\mathbb{R}$  such that  $\alpha \succeq \beta \iff \alpha \succ \beta$  or  $\alpha = \beta$  for  $\alpha, \beta \in \mathbb{R}$ . With (2) and (4),  $Q_v$  can be written as

$$Q_v(l, \mathbf{s}) = \begin{cases} 0, & \Phi_v(l, \mathbf{s}) \geq \gamma_1, \\ |\mathcal{R}| - 1, & \Phi_v(l, \mathbf{s}) < \gamma_{|\mathcal{R}|-1}, \\ k, & \gamma_k > \Phi_v(l, \mathbf{s}) \geq \gamma_{k+1}, 1 \leq k \leq |\mathcal{R}| - 2. \end{cases} \quad (6)$$

As shown in [34], the mappings  $Q_c$  and  $Q_v$  can both maximize the mutual information between  $X$  and the C2V (resp. V2C) message  $S$  (resp.  $R$ ). In addition, the mapping for bit decision  $Q_e : \mathcal{L} \times \mathcal{S}^{d_v} \rightarrow \mathcal{X}$  also needs to be designed in the MIM-QBP decoder, which is similar to the design of  $Q_v$  in the sense that the same RFs  $\phi_v$  and  $\phi_{ch}$  are used. However, the alphabet of the outgoing messages becomes  $\{\Phi_v(l, \mathbf{s}) : (l, \mathbf{s}) \in \mathcal{L} \times \mathcal{S}^{d_v}\}$  and we set  $|\Gamma_v| = |\mathcal{X}| - 1 = 1$  when quantizing  $\mathcal{B} \rightarrow \mathcal{X}$  for hard decision. We ignore the details here due to space limitation.

<sup>1</sup>The RFs, CFs, and TSs may or may not vary with iterations. Here we do not specify these notations with the associated iterations since once accomplishing the decoder design for one iteration, it is straightforward to generalize it for the other iterations.

### III. DESIGN OF MIM-QBP DECODING FOR IRREGULAR LDPC CODES

In this section, we extend the design principle of the MIM-QBP decoder to irregular LDPC codes and propose the generalized framework of the MIM-QBP decoder for the LDPC codes with arbitrary degree distributions. In particular, we derive the discrete DE for the MIM-QBP decoder and present the design of the node updates based on the discrete DE. Furthermore, we point out the connection between the MIM-QBP decoding for regular and irregular LDPC codes.

Denote  $\mathcal{D}_c = \{d_{c,1}, d_{c,2}, \dots, d_{c,\max}\}$  with  $d_{c,1} < d_{c,2} < \dots < d_{c,\max}$  and  $\mathcal{D}_v = \{d_{v,1}, d_{v,2}, \dots, d_{v,\max}\}$  with  $d_{v,1} < d_{v,2} < \dots < d_{v,\max}$  as the sets of the CN and VN degrees, respectively. An ensemble of binary LDPC codes can be characterized by the degree distributions as

$$\rho(x) = \sum_{i \in \mathcal{D}_c} \rho_i x^{i-1}, \quad \theta(x) = \sum_{j \in \mathcal{D}_v} \theta_j x^{j-1}, \quad (7)$$

where  $\rho_i$  and  $\theta_j$  are the fractions of edges incident to the CNs with degree- $i$  and the VNs with degree- $j$ , respectively. For convenience, let  $\mathcal{D}'_c = \{i-1 : i \in \mathcal{D}_c\}$  and  $\mathcal{D}'_v = \{j-1 : j \in \mathcal{D}_v\}$ . We denote  $\mathcal{U}^\mathcal{V} = \cup_{i \in \mathcal{V}} \mathcal{U}^i$  for any set  $\mathcal{U}$  and any integer set  $\mathcal{V}$ . In the following, we illustrate the design of the MIM-QBP decoder for irregular LDPC codes.

#### A. MIM-QBP Decoder Design at CN for Irregular LDPC Codes

According to (7), the outgoing edge connects to a degree- $i$  ( $i \in \mathcal{D}_c$ ) CN with probability  $\rho_i$ . Therefore, we have the vector of the incoming messages  $\mathbf{R} \in \mathcal{R}^{\mathcal{D}'_c}$ , where  $\dim(\mathbf{R}) = i \in \mathcal{D}'_c$  with probability  $\rho_{i+1}$ . For the CN update of the irregular LDPC codes, the C2V messages can be computed via the mapping:

$$Q_c : \mathcal{R}^{\mathcal{D}'_c} \rightarrow \mathcal{S},$$

where  $|\mathcal{D}'_c| = 1$  is a subcase for the regular LDPC codes. The design of  $Q_c$  is equivalent to solving the DMC quantization problem as shown in Fig. 2. Different from the case of the regular LDPC codes, we assume that the channel input bit  $X$  for the case of the irregular LDPC codes is transmitted over the sub-channel  $\text{Ch}_{d_{c,i}}$  with the corresponding probability  $\rho_{d_{c,i}}$ . Note that  $\text{Ch}_{d_{c,i}}$  refers to the sub-channel with  $d_c = d_{c,i}$  shown in Fig. 2. Since the sub-channel  $\text{Ch}_{d_{c,i}}$  is associated with the CNs of degree  $d_{c,i}$ , we can design  $Q_c$  in a similar way as the framework illustrated in Fig. 1. Based on (7), we consider the joint design of  $Q_c$  in the sense that the C2V message  $S$  is averaged over all incoming messages transmitted through each sub-channel  $\text{Ch}_{d_{c,i}}$  with probability  $\rho_{d_{c,i}}$ . The detailed design of the RF, CF, and TS for  $Q_c$  is presented as follows.

Define  $P_{X|R}$  as the probability of the channel input bit  $X$  conditioned on the V2C message  $R$ . For a realization  $r$  of  $R \in \mathcal{R}$ , the optimal RF  $\phi_c^*$  is selected as [34]

$$\phi_c^*(r) = \begin{cases} \text{sgn}(g(r))\epsilon, & |g(r)| = 1, \\ -\text{sgn}(g(r)) \log(|g(r)|), & \text{otherwise,} \end{cases} \quad (8)$$

where  $g(r) = P_{X|R}(0|r) - P_{X|R}(1|r)$  and  $\epsilon$  is a very small number to avoid  $|\phi_c^*(r)| = 0$ . Note that the computational

domain  $\mathbb{D}$  is  $\mathbb{R}$  for  $\phi_c^*$ , but  $\mathbb{D} = \mathbb{Z}$  is more preferable in practice. Therefore, we design  $\phi_c$  by linearly scaling  $\phi_c^*$  with rounding, which converts  $\mathbb{D}$  from  $\mathbb{R}$  to  $\mathbb{Z}$ . Denote the scaling factor by  $\alpha = |\phi_c|_{\max} / |\phi_c^*|_{\max}$ , where  $|\phi_c|_{\max}$  is the maximum allowed absolute value of  $\phi_c(\cdot)$  and  $|\phi_c^*|_{\max} = \max\{|\phi_c^*(r)| : r \in \mathcal{R}, g(r) \neq 0\}$ . According to (1), we set  $|\phi_c|_{\max} = \lfloor (2^{q_c-1} - 1) / d_{c,\max} \rfloor$  such that  $\sum_{k=1}^{d_{c,\max}} |\phi_c(r_k)|$  does not overflow with the integer value  $2^{q_c-1} - 1$  when computing the outgoing message by  $\Phi_c$  (one bit is needed for computing the sign). Then the RF  $\phi_c$  for the CN update is given by

$$\phi_c(r) = \begin{cases} \text{sgn}(g(r)) \cdot \max\{1, \lfloor \alpha \cdot \phi_c^*(r) + 0.5 \rfloor\}, & g(r) \neq 0, \\ |\phi_c|_{\max}, & g(r) = 0. \end{cases} \quad (9)$$

As proved in [34], with  $\phi_c = \eta \phi_c^*$ , where  $\eta$  is a positive number,  $Q_c$  defined by (5) can maximize the mutual information between  $X$  and the C2V message  $S$  among all the functions mapping  $\mathcal{R}^{d_c-1}$  to  $\mathcal{S}$  for regular LDPC codes. By replacing  $\mathcal{R}^{d_c-1}$  with  $\mathcal{R}^{\mathcal{D}'_c}$ , it is easy to obtain the same conclusion for the irregular LDPC codes. This means that the RF defined by (9) can make  $Q_c$  achieve information optimum when  $q_c$  is large enough.

As depicted in Fig. 2, each sub-channel has  $i$  ( $i \in \mathcal{D}'_c$ ) incoming messages corresponding to its associated CN degree. For  $i \geq 1$ , we denote the vector of incoming messages by  $\mathbf{R} \in \mathcal{R}^i$ . Let  $\mathcal{A}_i = \{a_{i,1}, a_{i,2}, \dots, a_{i,|\mathcal{A}_i|}\} = \{\Phi_c(\mathbf{r}) : \mathbf{r} \in \mathcal{R}^i\}$  be the alphabet of the outgoing message for the sub-channel with  $i$  incoming messages, where  $\Phi_c(\cdot)$  is given by (1). To design  $Q_c$  for each sub-channel, we adopt the discrete DE and trace the joint distribution  $P_{\mathbf{R}|X}$  of  $\mathbf{R}$  conditioned on the channel input bit  $X$  by

$$P_{\mathbf{R}|X}(\mathbf{r}|x) = \left(\frac{1}{2}\right)^{\dim(\mathbf{r})-1} \sum_{\mathbf{x} : \oplus \mathbf{x} = x} \prod_{k=1}^{\dim(\mathbf{r})} P_{R_k|X}(r_k|x_k), \quad (10)$$

where  $x \in \mathcal{X}$  is a realization of  $X$ ,  $\mathbf{x} = (x_1, x_2, \dots, x_{d_c-1}) \in \mathcal{X}^{d_c-1}$  is the vector of channel input bits associated with its connecting VNs, and  $\oplus \mathbf{x} = x_1 \oplus x_2 \oplus \dots \oplus x_{d_c-1}$  with  $\oplus$  operating as the addition in GF(2). Denoted by  $A_i$ , a random variable taking values from  $\mathcal{A}_i$ . The probability of the random variable  $A_i$  conditioned on the channel input bit  $X$ , i.e.,  $P_{A_i|X}$  is given by

$$P_{A_i|X}(a_{i,k}|x) = \sum_{\mathbf{r} \in \mathcal{R}^i, \Phi_c(\mathbf{r}) = a_{i,k}} P_{\mathbf{R}|X}(\mathbf{r}|x), \quad k = 1, 2, \dots, |\mathcal{A}_i|. \quad (11)$$

Define  $A \in \mathcal{A}$  as the random variable of the outgoing message for all sub-channels. Denoted by  $P_{A|X}$ , the probability of  $A$  conditioned on the channel input bit  $X$ . By considering the probability of  $X$  transmitted through each sub-channel, we have

$$\mathcal{A} = \cup_{i \in \mathcal{D}'_c} \mathcal{A}_i, \quad P_{A|X}(a|x) = \sum_{i \in \mathcal{D}'_c} \rho_{i+1} \cdot P_{A_i|X}(a|x), \quad (12)$$

where  $a$  is a realization of  $A \in \mathcal{A}$ . Note that one advantage of the MIM-QBP decoder is that  $\mathcal{A}$  can be computed by handling all  $\mathcal{A}_i$  ( $i \in \mathcal{D}'_c$ ) simultaneously with the DMC quantization model shown in Fig. 2. Assume that a realization  $\mathbf{r}$  of

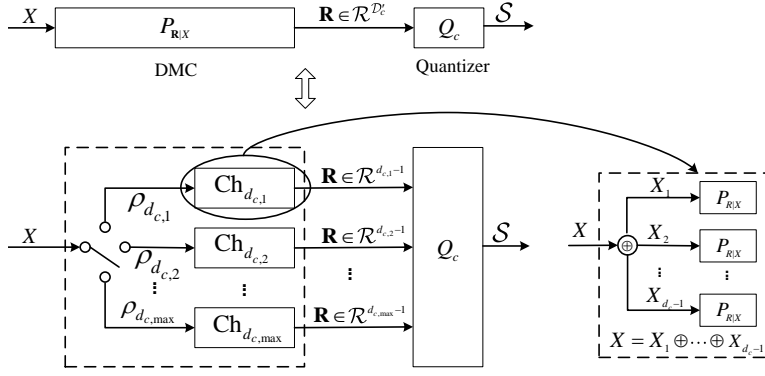


Fig. 2: The MIM-QBP decoder design at CN and its equivalence to quantization for DMC.

$\mathbf{R} \in \mathcal{R}^{D'_c}$  is transmitted through the DMC with probability  $\rho_{\dim(\mathbf{r})+1}$ . The joint distribution of the incoming messages  $\mathbf{R} \in \mathcal{R}^{D'_c}$  at a CN is equivalent to the channel transition probability  $P_{\mathbf{R}|X}(\mathbf{r}|x)$  of the DMC. According to (7) and (10),  $P_{\mathbf{R}|X}$  is derived as

$$P_{\mathbf{R}|X}(\mathbf{r}|x) = \rho_{\dim(\mathbf{r})+1} \left(\frac{1}{2}\right)^{\dim(\mathbf{r})-1} \cdot \sum_{\mathbf{x}: \oplus \mathbf{x} = x} \prod_{k=1}^{\dim(\mathbf{r})} P_{R|X}(r_k|x_k). \quad (13)$$

With (12) and (13), we demonstrate the relationship between the design of  $Q_c$  for each sub-channel and the equivalent DMC as

$$\begin{aligned} \mathcal{A} = \cup_{i \in \mathcal{D}'_c} \mathcal{A}_i, \quad P_{A|X}(a|x) &= \sum_{i \in \mathcal{D}'_c} \rho_{i+1} \cdot P_{A_i|X}(a|x) \\ &= \sum_{\substack{\mathbf{r} \in \mathcal{R}^{D'_c} \\ \Phi_c(\mathbf{r}) = a}} P_{\mathbf{R}|X}(\mathbf{r}|x). \end{aligned} \quad (14)$$

Based on  $\mathcal{A}$  and  $P_{A|X}$ , we can compute the optimal SDQ  $\Lambda_c$  by DP [36] to generate  $\Gamma_c$  as defined by (3), and  $Q_c$  can be obtained from (5). Meanwhile, for a realization  $s$  of the C2V message  $S \in \mathcal{S}$ , we can compute the probability of  $S$  conditioned on the channel input bit  $X$ , i.e.,  $P_{S|X}$ , as

$$P_{S|X}(s|x) = \sum_{k=\lambda_s+1}^{\lambda_{s+1}} P_{A|X}(a_k|x). \quad (15)$$

### B. MIM-QBP Decoder Design at VN for Irregular LDPC Codes

According to (7), the outgoing edge connects to a degree- $j$  ( $j \in \mathcal{D}_v$ ) VN with probability  $\theta_j$ . Thus, the vector of the incoming messages  $(L, \mathbf{S}) \in \mathcal{L} \times \mathcal{S}^{D'_v}$  has  $\dim(\mathbf{S}) = j \in \mathcal{D}'_v$  with probability  $\theta_{j+1}$ . For the VN update of irregular LDPC codes, the V2C messages can be calculated via the mapping:

$$Q_v : \mathcal{L} \times \mathcal{S}^{D'_v} \rightarrow \mathcal{R},$$

where we have  $|\mathcal{D}'_v| = 1$  for regular LDPC codes as a subcase. As shown by Fig. 3, the design of  $Q_v$  is equivalent to solve the quantization problem over DMC. Similar to the case of the CN update, the channel input bit  $X$  is transmitted over the sub-channel  $\text{Ch}_{d_{v,j}}$  with probability  $\theta_{d_{v,j}}$ . Note that  $\text{Ch}_{d_{v,j}}$  refers to the sub-channel with  $d_v = d_{v,j}$  shown in Fig. 3. As each

sub-channel  $\text{Ch}_{d_{v,j}}$  is associated with the VNs of degree  $d_{v,j}$ , we follow the framework illustrated in Fig. 1 to design the mapping  $Q_v$  by utilizing similar principles for the VN update as in [34]. We consider the joint design of  $Q_v$  such that the V2C message  $R$  is the average of all incoming messages from each sub-channel  $\text{Ch}_{d_{v,j}}$  with probability  $\theta_{d_{v,j}}$ . The design of the RFs, CF, and TS for  $Q_v$  is presented in details as follows.

Define  $P_{L|X}$  as the probability of the channel output  $L$  conditioned on the channel input bit  $X$ . For a realization  $s$  of C2V message  $S \in \mathcal{S}$  and a realization  $l$  of channel output  $L \in \mathcal{L}$ , we choose the optimal RFs  $\phi_v^*$  and  $\phi_{ch}^*$  as [34]

$$\begin{cases} \phi_v^*(s) = \log(P_{S|X}(s|0)/P_{S|X}(s|1)), \\ \phi_{ch}^*(l) = \log(P_{L|X}(l|0)/P_{L|X}(l|1)). \end{cases} \quad (16)$$

For practical concerns,  $\phi_v(s)$  and  $\phi_{ch}(l)$  are also designed in  $\mathbb{Z}$  by linearly scaling  $\phi_v^*(s)$  and  $\phi_{ch}^*(l)$  with rounding. We set the scaling factor for both  $\phi_v(\cdot)$  and  $\phi_{ch}(\cdot)$  as  $\beta = |\phi_{v,ch}|_{\max}/|\phi_{v,ch}^*|_{\max}$ . Note that  $|\phi_{v,ch}|_{\max}$  is the maximum allowable absolute value for  $\phi_v(\cdot)$  and  $\phi_{ch}(\cdot)$ , and  $|\phi_{v,ch}^*|_{\max} = \max(\{|\phi_v^*(s)| : s \in \mathcal{S}\} \cup \{|\phi_{ch}^*(l)| : l \in \mathcal{L}\})$ . Based on (2), we set  $|\phi_{v,ch}|_{\max} = \lfloor (2^{q_v} - 1)/(d_{v,\max} + 1) \rfloor$  to ensure that  $|\phi_{ch}(l)| + d_{v,\max}|\phi_v(s)|$  does not exceed  $2^{q_v} - 1$  for  $\forall l \in \mathcal{L}$  and  $\forall s \in \mathcal{S}$ . As a result, the RFs for the VN update are given by

$$\begin{cases} \phi_v(s) = \text{sgn}(\phi_v^*(s)) \cdot \lfloor \beta \cdot |\phi_v^*(s)| + 0.5 \rfloor, \\ \phi_{ch}(l) = \text{sgn}(\phi_{ch}^*(l)) \cdot \lfloor \beta \cdot |\phi_{ch}^*(l)| + 0.5 \rfloor. \end{cases} \quad (17)$$

It is proved in [34] that with  $\phi_v = \eta\phi_v^*$  and  $\phi_{ch} = \eta\phi_{ch}^*$  for a positive number  $\eta$ ,  $Q_v$  defined by (6) can maximize the mutual information between  $X$  and the V2C message  $R$  among all the functions mapping  $\mathcal{L} \times \mathcal{S}^{d_v-1}$  to  $\mathcal{R}$  for regular LDPC codes. For irregular LDPC codes, the same conclusion can be drawn by substituting  $\mathcal{L} \times \mathcal{S}^{d_v-1}$  with  $\mathcal{L} \times \mathcal{S}^{D'_v}$ . This indicates that the RFs defined by (17) lead to an information optimum  $Q_v$  with sufficiently large  $q_v$ .

As illustrated in Fig. 3, each sub-channel has  $j+1$  ( $j \in \mathcal{D}'_v$ ) incoming messages, where one is from the channel output and the others are from the  $j$  neighboring CNs. For  $j \geq 0$ , we define the vector of incoming messages from the  $j$  neighboring CNs as  $\mathbf{S} \in \mathcal{S}^j$ . Let  $\mathcal{B}_j = \{b_{j,1}, b_{j,2}, \dots, b_{j,|\mathcal{B}_j|}\} = \{\Phi_v(l, \mathbf{s}) : l \in \mathcal{L}, \mathbf{s} \in \mathcal{S}^j\}$  be the alphabet of the extrinsic messages for the sub-channel with incoming messages  $(L, \mathbf{S}) \in \mathcal{L} \times \mathcal{S}^j$ ,

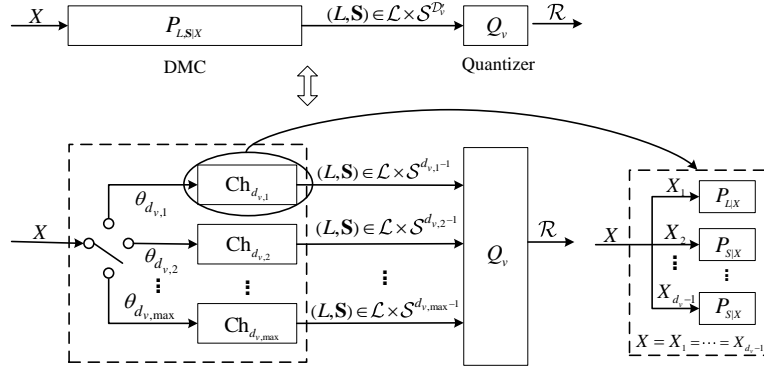


Fig. 3: The MIM-QBP decoder design at VN and its equivalence to quantization for DMC.

where  $\Phi_v(\cdot)$  is given by (2) and  $\Phi_v(l, s) = \phi_{ch}(l)$  for  $j = 0$ . To design  $Q_v$  for each sub-channel based on the discrete DE, we track the joint distribution  $P_{L,S|X}$  of  $(L, \mathbf{S})$  conditioned on the channel input bit  $X$  by

$$P_{L,S|X}(l, \mathbf{s}|x) = P_{L|X}(l|x) \prod_{k=1}^{\dim(\mathbf{s})} P_{S|X}(s_k|x).$$

Note that we have  $P_{L,S|X}(l, \mathbf{s}|x) = P_{L|X}(l|x)$  when  $j = 0$ . Define  $B_j$  as a random variable taking values from  $\mathcal{B}_j$ . The conditional probability  $P_{B_j|X}$  can be computed by

$$P_{B_j|X}(b_{j,k}|x) = \sum_{\substack{(l, \mathbf{s}) \in \mathcal{L} \times \mathcal{S}^j \\ \Phi_v(l, \mathbf{s}) = b_{j,k}}} P_{L,S|X}(l, \mathbf{s}|x), \quad k = 1, 2, \dots, |\mathcal{B}_j|.$$

Define  $B \in \mathcal{B}$  as the random variable of the outgoing message among all sub-channels. Denoted by  $P_{B|X}$ , the probability of  $B$  conditioned on the channel input bit  $X$ . With the probability of  $X$  being transmitted through each sub-channel, we obtain

$$\mathcal{B} = \cup_{j \in \mathcal{D}'_v} \mathcal{B}_j, \quad P_{B|X}(b|x) = \sum_{j \in \mathcal{D}'_v} \theta_{j+1} \cdot P_{B_j|X}(b|x), \quad (18)$$

where  $b \in \mathcal{B}$  is a realization of the outgoing message among all sub-channels. Owing to the DMC quantization model shown in Fig. 3, we can also obtain  $\mathcal{B}$  by considering all  $\mathcal{B}_j$ , ( $j \in \mathcal{D}'_v$ ) at the same time. Suppose that a realization  $(l, \mathbf{s})$  of  $(L, \mathbf{S}) \in \mathcal{L} \times \mathcal{S}^{D'_v}$  is transmitted over the DMC with probability  $\theta_{\dim(\mathbf{s})+1}$ . The joint distribution of incoming messages  $(L, \mathbf{S}) \in \mathcal{L} \times \mathcal{S}^{D'_v}$  at a VN is equivalent to the channel transition probability  $P_{L,S|X}(l, \mathbf{s}|x)$  of the DMC. Therefore, we have

$$P_{L,S|X}(l, \mathbf{s}|x) = \theta_{\dim(\mathbf{s})+1} P_{L|X}(l|x) \prod_{k=1}^{\dim(\mathbf{s})} P_{S|X}(s_k|x). \quad (19)$$

To point out the relationship between the design of  $Q_v$  for each sub-channel and the equivalent DMC, we rewrite (18) and (19) as

$$\begin{aligned} \mathcal{B} = \cup_{j \in \mathcal{D}'_v} \mathcal{B}_j, \quad P_{B|X}(b|x) &= \sum_{j \in \mathcal{D}'_v} \theta_{j+1} \cdot P_{B_j|X}(b|x) \\ &= \sum_{\substack{(l, \mathbf{s}) \in \mathcal{L} \times \mathcal{S}^{D'_v} \\ \Phi_v(l, \mathbf{s}) = b}} P_{L,S|X}(l, \mathbf{s}|x). \end{aligned} \quad (20)$$

Based on  $\mathcal{B}$  and  $P_{B|X}$ , the optimal SDQ  $\Lambda_v$  can be obtained by the DP method [36], which generates  $\Gamma_v$  as in (4). After that,  $Q_v$  can be computed by (6). For a realization  $r$  of the V2C message  $R \in \mathcal{R}$ , the probability of  $R$  conditioned on the channel input bit  $X$ , i.e.,  $P_{R|X}$ , is computed by

$$P_{R|X}(r|x) = \sum_{k=\lambda_r+1}^{\lambda_r+1} P_{B|X}(b_k|x). \quad (21)$$

In addition, the mapping for the bit decision is  $Q_e : \mathcal{L} \times \mathcal{S}^{D'_v} \rightarrow \mathcal{X}$ . Since the design of  $Q_e$  is similar to that of  $Q_v$ , we ignore the details to save the space.

### C. Comparison with the Prior Art Decoder Designs

We now discuss the difference between the design of the MIM-QBP decoder and the LUT decoder variants in [29]–[31], [35] for irregular LDPC codes. In [29]–[31], [35], the design of the MIM-LUT decoders for irregular LDPC codes can also be related to Figs. 2 and 3, where each sub-channel represents a CN or VN with a specific degree. In [29]–[31], the LUTs for node updates are constructed by two steps. Firstly, the LUT for each sub-channel is designed individually according to its associated degree, where the decomposition technique [27] is employed to avoid memory overflow. After that, a joint design is considered over all sub-channels labeled by “ $\text{Ch}_{d_{e,i}}$ ” or “ $\text{Ch}_{d_{v,j}}$ ” to obtain the LUT of the output alphabet such as  $\mathcal{S}$  or  $\mathcal{R}$  with a manageable size. More specifically, the message alignment method is utilized in [29] as a post-processing step to jointly design the output LUT after the individual design. The min-LUT decoder proposed in [31] designs the output LUT for the VN update based on a binary tree structure with  $j$  levels, which is called the  $j$ -level LUT tree with  $j \in \mathcal{D}'_v$ . At the first  $j-1$  levels of the LUT tree, individual design is conducted by cascading two input LUTs at each level to generate an intermediate LUT with a higher dimension. Therefore, a series of intermediate LUTs are obtained from the individual design. Based on these LUTs, the joint design of the output LUT is performed on the  $j$ -th level of the LUT tree by considering the degree distribution of the VNs. Note that the design method in [31] is equivalent to the approach known as the implicit message alignment [30], in the sense of the way of taking the contribution of degree distributions into account for different sub-channels.

Obviously, the design methods in [29]–[31] result in various intermediate LUTs for different sub-channels. Moreover, the individual design deteriorates the performance of the MIM-LUT decoders since table decomposition causes the loss of mutual information [33]. Compared to the MIM-LUT decoders described above, the MIM-QBP decoder adopts the same RFs and TSs for different sub-channels, i.e., for updating the nodes with different degrees. This simplifies the decoder design as it only requires the parameters  $q_m$ ,  $q_c$ , and  $q_v$ . Furthermore, the output alphabet  $\mathcal{R}^{\mathcal{D}'_c}$  or  $\mathcal{L} \times \mathcal{S}^{\mathcal{D}'_v}$  for all sub-channels is handled simultaneously without causing any storage problem since all the incoming messages are reconstructed and processed in the computational domain. In this case, the MIM-QBP decoder is equivalent to the MIM-LUT decoder designed without table decomposition, which avoids the degradation of the error performance.

Apart from the above MIM-LUT decoders, Wang et al. proposed the RCQ decoder in [35] to overcome the high memory requirement of the MIM-LUT decoders. The design of the RCQ decoder is also performed similarly to that of the MIM-QBP decoder, which considers the joint design of all sub-channels at the same time. In particular, each incoming message is mapped to a corresponding LLR value by the RFs. Then the extrinsic messages are computed based on either the BP or the MS algorithm. A hierarchical dynamic quantization (HDQ) scheme is performed on the extrinsic messages to obtain the LUTs of the outgoing messages. Nevertheless, the RFs of the RCQ decoder is based on floating-pointing precision so that it requires additional uniform quantizer when the RCQ decoder operates with finite precision. On the contrary, the RFs of our proposed MIM-QBP decoder perform directly on integer domain  $\mathbb{Z}$ , which simplifies the design process. Furthermore, the HDQ scheme is a sub-optimal quantization because it can only optimize the TS sequentially instead of searching the optimal TS globally. In contrast, our proposed MIM-QBP decoder adopts the DP method in [36], which is proved to be optimal [34].

#### IV. THE MIM-QMS DECODING WITH MAX-PRODUCT OPERATION

Compared to the precision of the extrinsic messages  $q_m$ , it is shown in [34] that we need to set a large  $q_c$  for  $\Phi_c$  based on the BP algorithm to compute the alphabet of the outgoing message. Moreover, the CF  $\Phi_c$  based on (1) requires numerous fix-point additions especially when decoding the LDPC codes with high CN degrees. These requirements result in a high resource consumption and computational complexity. To reduce the resource consumption and the decoding complexity, we approximate the CN update of the MIM-QBP decoder by the MS algorithm [31], which leads to the MIM-QMS decoder. Moreover, a max-product operation is proposed in this section to implement the MS algorithm efficiently. We also introduce a fast computation method to trace the conditional probability of the C2V message for the discrete DE, which simplifies the design of the decoder. In the following, we first present the details of the max-product operation.

Denoted by  $\mathcal{Y} = \{y_0, y_1, \dots, y_{|\mathcal{Y}|-1}\}$ , a finite alphabet with  $|\mathcal{Y}| = 2^{q_m}$ . We refer  $\neg$  to the symbol inversion operation such

that  $\neg y_k = y_{|\mathcal{Y}|-1-k}$  for  $\forall y_k \in \mathcal{Y}, k = 0, 1, \dots, |\mathcal{Y}| - 1$ . For a realization  $\mathbf{r}$  of  $\mathbf{R} \in \mathcal{R}^{\mathcal{D}'_c}$ , the CF based on the max-product operation performs as

$$\Phi_c(\mathbf{r}) = \begin{cases} \arg \max_{k=1,2,\dots,\dim(\mathbf{r})} (\text{abs}(r_k)), & \prod_{k=1}^{\dim(\mathbf{r})} \text{sign}(r_k) = 1, \\ \neg \arg \max_{k=1,2,\dots,\dim(\mathbf{r})} (\text{abs}(r_k)), & \prod_{k=1}^{\dim(\mathbf{r})} \text{sign}(r_k) = -1. \end{cases} \quad (22)$$

Note that  $\text{sign}(\cdot)$  and  $\text{abs}(\cdot)$  in (22) refer to the sign and magnitude of a symbol, respectively. Particularly, for a symbol  $y \in \mathcal{Y}$ , we have

$$\text{sign}(y) = \begin{cases} 1, & y \in [0, 2^{q_m-1} - 1], \\ -1, & y \in [2^{q_m-1}, 2^{q_m} - 1], \end{cases} \quad (23)$$

and

$$\text{abs}(y) = \begin{cases} y, & y \in [0, 2^{q_m-1} - 1], \\ 2^{q_m} - y - 1, & y \in [2^{q_m-1}, 2^{q_m} - 1]. \end{cases} \quad (24)$$

To distinguish the CFs represented by (1) and (22), we denote the CF based on the BP algorithm by  $\Phi_c^{\text{BP}}$  and denote the CF based on the MS algorithm by  $\Phi_c^{\text{MS}}$  in the rest of this paper. We call the decoder designed based on  $\Phi_c^{\text{MS}}$  as the mutual information-maximizing quantized MS (MIM-QMS) decoder. Note that the symbols exchanged within the decoder in [31] are associated to the LLR values and sorted according to the ascending order of the LLR values. Compared to [31], our proposed MIM-QMS decoder arranges the symbols in descending order of their associated LLRs as shown in [34]. This is the reason that we use  $\max(\cdot)$  in (22) instead of the min update.

With the max-product operation, the reconstruction and the calculation steps in the CN update are not required for the MIM-QMS decoder. Therefore, the conditional probability  $P_{S|X}$  can be directly derived from  $P_{\mathbf{R}|X}$  as

$$P_{S|X}(s|x) = \sum_{\mathbf{r} \in \mathcal{R}^{\mathcal{D}'_c}, \Phi_c^{\text{MS}}(\mathbf{r})=s} P_{\mathbf{R}|X}(\mathbf{r}|x), \quad (25)$$

where  $P_{\mathbf{R}|X}$  is given by (13). However, computing (25) has a prohibitively high computational complexity when  $|\mathcal{R}^{\mathcal{D}'_c}|$  is large. Here we propose a fast method to calculate  $P_{S|X}$  in a more efficient way. Similar to (25), for the vector of the  $i$  incoming messages  $\mathbf{R} \in \mathcal{R}^i$  ( $i \geq 1$ ), we define  $\delta_i^{\pm}(\cdot)$  and  $\delta_i^-(\cdot)$  as

$$\begin{aligned} \delta_i^{\pm}(s) &= P_{S|X}(s|0) \pm P_{S|X}(s|1) \\ &= \sum_{\mathbf{r} \in \mathcal{R}^i, \Phi_c^{\text{MS}}(\mathbf{r})=s} (P_{\mathbf{R}|X}(\mathbf{r}|0) \pm P_{\mathbf{R}|X}(\mathbf{r}|1)). \end{aligned}$$

For  $i = 1$ , we have  $\Phi_c^{\text{MS}}(r) = s$  so that

$$\delta_1^{\pm}(s) = P_{R|X}(r|0) \pm P_{R|X}(r|1).$$

For  $i > 1$ , the  $i$  incoming messages are handled one by one as

$$\delta_i^{\pm}(s) = \sum_{\substack{r \in \mathcal{R}, s' \in \mathcal{S} \\ \Phi_c(r, s')=s}} \frac{1}{2} (P_{R|X}(r|0) \pm P_{R|X}(r|1)) \cdot \delta_{i-1}^{\pm}(s'),$$

where  $s' \in \mathcal{S}$  is the symbol computed by (22) with  $i - 1$  incoming messages, and  $(r, s')$  is the vector of incoming messages with dimension  $\dim(r, s') = 2$ . The corresponding computation of  $P_{S|X}$  is summarized in **Algorithm 1**.

---

**Algorithm 1** Computation of  $P_{S|X}$ 


---

**Input:**  $P_{R|X}, \rho(x), d_{c,\max}$ .

**Output:**  $P_{S|X}$ .

- 1: Set  $P_{S|X}(s|0) = P_{S|X}(s|1) = 0$ ,  
 $\delta_i^\pm(\cdot) = 0$  for  $i = 1, 2, \dots, d_{c,\max} - 1$
  - 2: **for**  $\forall r \in \mathcal{R}$  and each  $r = s \in \mathcal{S}$  **do**
  - 3:   Compute  $\delta_1^\pm(s) = P_{R|X}(r|0) \pm P_{R|X}(r|1)$
  - 4: **end for**
  - 5: **for**  $i = 2 : d_{c,\max} - 1$  **do**
  - 6:   **for**  $\forall r \in \mathcal{R}$  and  $\forall s' \in \mathcal{S}$  **do**
  - 7:     Perform  $s = \Phi_c^{\text{MS}}(r, s')$  as (22)
  - 8:     Compute
  - 9:      $\delta_i^\pm(s) = \frac{1}{2}(P_{R|X}(r|0) \pm P_{R|X}(r|1)) \cdot \delta_{i-1}^\pm(s')$
  - 10:   **end for**
  - 11: **end for**
  - 12: **for**  $\forall s \in \mathcal{S}$  and each  $i \in \mathcal{D}'_c$  **do**
  - 13:    $P_{S|X}(s|0) = \frac{\delta_i^+(s) + \delta_i^-(s)}{2} \cdot \rho_{i+1}$
  - 14:    $P_{S|X}(s|1) = \frac{\delta_i^+(s) - \delta_i^-(s)}{2} \cdot \rho_{i+1}$
  - 15: **end for**
  - 16: **return**  $P_{S|X}$
- 

Compared to the MIM-QBP decoder, we will show in the next section that the MIM-QMS decoder is simplified by the above fast computation method and there is also a much less computational complexity when performing the MIM-QMS decoder. More importantly, the number of bits used for computing  $\Phi_c(\cdot)$  is equal to that used for representing the incoming messages, i.e.,  $q_c = q_m$ , for all iterations. Therefore, the MIM-QMS decoder has a much less resource consumption than the MIM-QBP decoder, and the precision of the MIM-QMS decoder can be simply determined by  $q_m$  and  $q_v$ . In the remaining of this paper, we call either the MIM-QBP decoder or the MIM-QMS decoder as the MIM quantized decoder.

## V. PRACTICAL ASPECTS OF MIM QUANTIZED DECODER

In this section, we discuss the practical aspects that need to be considered in the design of the MIM quantized decoder. We introduce the channel quantization and the choice of a proper operating threshold for the MIM quantized decoder, which substantially affects the decoder's error performance. We further optimize the VN update by a dynamic reconstruction method, which can make a full use of the allocated bits for different iterations without degrading the precision of the decoder. In addition, we present the hardware architectures for the node updates of the MIM-QBP decoder and analyze the design and decoding complexity of the MIM quantized decoder.

### A. Operating Threshold

Given the parameters  $q_m, q_c, q_v$  and the maximum decoding iterations, the performance of the MIM quantized decoder is related to the channel transition probability  $P_{L|X}$  of the DMC. To obtain a DMC, we consider the channel quantization on a binary-input additive white Gaussian noise channel (AWGNC). Define  $y \in \mathbb{R}$  as the continuous channel output of the binary-input AWGNC. We first uniformly quantize  $y$  to  $N$  discrete outputs. Then the channel quantizer  $Q_{ch}$  on  $y$  is obtained by the DP method in [36], which aims to maximize the mutual information between the channel input  $X$  and the DMC output  $L$  such that [23]

$$Q_{ch} = \arg \max_Q I(X; L).$$

Denoted by  $\Gamma_{ch}$ , the TS for the channel quantization is given by  $\Gamma_{ch} = \{\gamma_k : k = 1, 2, \dots, 2^{q_m} - 1\}$ , where  $\gamma_1 < \gamma_2 < \dots < \gamma_{2^{q_m} - 1}$ . Therefore, for any continuous channel output  $y \in \mathbb{R}$ , its quantization output is

$$Q_{ch}(y) = \begin{cases} 1, & y \leq \gamma_1, \\ 2^{q_m} - 1, & y > \gamma_{2^{q_m} - 1}, \\ i, & \gamma_{i-1} < y \leq \gamma_i, 1 < i < 2^{q_m} - 1. \end{cases} \quad (26)$$

For a binary-input AWGNC,  $P_{L|X}$  is essentially determined by the associated noise standard deviation  $\sigma_d$ . We call  $\sigma_d$  the operating threshold for the MIM quantized decoder. To design the MIM quantized decoder, it is necessary to carefully select the operating threshold  $\sigma_d$ . Our simulation results show that a proper choice of  $\sigma_d$  is around the decoding threshold  $\sigma^*$  of the LDPC codes, as it can make the mutual information between the channel input  $X$  and the V2C message  $R$  approach 1 with the maximum decoding iteration. This is consistent with the results investigated empirically in [27]–[31], [34]. After selecting  $\sigma_d$ , the design approach described in Section III can be conducted off-line to find the RFs (i.e.,  $\phi_{ch}, \phi_c$ , and  $\phi_v$ ) and the TSs (i.e.,  $\Gamma_{ch}, \Gamma_c$ , and  $\Gamma_v$ ) for the MIM quantized decoder. The mappings  $Q_c, Q_v$ , and  $Q_e$  can then be determined based on the RFs and TSs afterwards.

### B. Dynamic Reconstruction

From (17), we observed that  $|\phi_{ch}|_{\max} + d_{v,\max}|\phi_v|_{\max}$  can be much smaller than  $2^{q_v} - 1$  especially for initial decoding iterations, where  $|\phi_v|_{\max} = \max\{|\phi_v(s)| : s \in \mathcal{S}\}$  and  $|\phi_{ch}|_{\max} = \max\{|\phi_{ch}(l)| : l \in \mathcal{L}\}$ . In this case, the precision of the designed decoder is reduced since the reconstructed values for the VN update do not make a full use of  $q_v$  bits. The reason is that  $|\phi_{v,ch}|_{\max}$  is set to a fixed value for all iterations and  $|\phi_v^*(s)|$  computed by (16) is much smaller than  $|\phi_{v,ch}^*|_{\max}$  at the beginning of decoding. Thus,  $\phi_v(s)$  reconstructed by (17) has a small magnitude and results in  $|\phi_{ch}(l)| + d_{v,\max}|\phi_v(s)| \ll 2^{q_v} - 1$ .

To solve this problem, we propose a dynamic reconstruction method to optimize the design of the VN update, where the scaling factor for  $\phi_v(s)$  and  $\phi_{ch}(l)$  is adjusted for different iterations to fully utilize the  $q_v$  bits. We summarize the dynamic reconstruction method in **Algorithm 2**. Note that the scaling factor in the dynamic reconstruction method is



---

**Algorithm 2** Dynamic Reconstruction
 

---

**Input:**  $\phi_v^*(s)$ ,  $\phi_{ch}^*(l)$  given by (16).

**Output:**  $\phi_v(s)$ ,  $\phi_{ch}(l)$ .

 1: **Initialize:**

$$|\phi_{v,ch}|_{\text{low}} = (2^{q_v} - 1)/(d_{v,\text{max}} + 1)$$

$$|\phi_{v,ch}|_{\text{upp}} = 2^{q_v - 1}$$

 2: Find  $|\phi_{v,ch}^*|_{\text{max}} = \max(\{|\phi_v^*(s)| : s \in \mathcal{S}\} \cup \{|\phi_{ch}^*(l)| : l \in \mathcal{L}\})$ 

 3: **while**  $|\phi_{v,ch}|_{\text{low}} + 1 < |\phi_{v,ch}|_{\text{upp}}$  **do**

 4:  $|\phi_{v,ch}|_{\text{tmp}} = \frac{1}{2}(|\phi_{v,ch}|_{\text{low}} + |\phi_{v,ch}|_{\text{upp}})$ 

 5:  $\hat{\beta} = |\phi_{v,ch}|_{\text{tmp}} / |\phi_{v,ch}^*|_{\text{max}}$ 

 6: **for**  $\forall s \in \mathcal{S}$  and  $\forall l \in \mathcal{L}$  **do**

 7: Compute  $|\phi_v(s)|_{\text{tmp}} = \lfloor \hat{\beta} \cdot |\phi_v^*(s)| + 0.5 \rfloor$ 

 8: Compute  $|\phi_{ch}(l)|_{\text{tmp}} = \lfloor \hat{\beta} \cdot |\phi_{ch}^*(l)| + 0.5 \rfloor$ 

 9: **end for**

 10: Update  $|\phi_v|_{\text{max}} = \max\{|\phi_v(s)|_{\text{tmp}} : s \in \mathcal{S}\}$ 

 11: Update  $|\phi_{ch}|_{\text{max}} = \max\{|\phi_{ch}(l)|_{\text{tmp}} : l \in \mathcal{L}\}$ 

 12: **if**  $|\phi_{ch}|_{\text{max}} + d_{v,\text{max}}|\phi_v|_{\text{max}} \leq 2^{q_v} - 1$  **then**

 13:  $|\phi_{v,ch}|_{\text{low}} = |\phi_{v,ch}|_{\text{tmp}}$ 

 14: **else**

 15:  $|\phi_{v,ch}|_{\text{upp}} = |\phi_{v,ch}|_{\text{tmp}}$ 

 16: **end if**

 17: **end while**

 18:  $\beta = |\phi_{v,ch}|_{\text{low}} / |\phi_{v,ch}^*|_{\text{max}}$ 

 19: Set  $\phi_v(s) = \text{sgn}(\phi_v^*(s)) \cdot \lfloor \beta \cdot |\phi_v^*(s)| + 0.5 \rfloor$ 

 20: Set  $\phi_{ch}(l) = \text{sgn}(\phi_{ch}^*(l)) \cdot \lfloor \beta \cdot |\phi_{ch}^*(l)| + 0.5 \rfloor$ 

 21: **return**  $\phi_v(s)$  and  $\phi_{ch}(l)$ 


---

determined based on bisection search of  $|\phi_{v,ch}|_{\text{max}}$ . This makes  $|\phi_{ch}|_{\text{max}} + d_{v,\text{max}}|\phi_v|_{\text{max}}$  as close to  $2^{q_v} - 1$  as possible so that the precision of the decoder can remain unchanged for all iterations.

### C. Complexity Analysis

In practical implementations, the computational complexity of the MIM quantized decoder is a critical issue. We first discuss the computational complexity of designing the MIM-QBP decoder for irregular LDPC codes. For the node updates of the MIM-QBP decoder, the computational complexity is divided into two parts, i.e., calculating the alphabet of the outgoing message ( $\mathcal{A}$  or  $\mathcal{B}$ ) and finding the TS ( $\Gamma_c$  or  $\Gamma_v$ ). In the design of the CN update, we can adopt **Algorithm 1** proposed in [34] to compute  $\mathcal{A}$ . As shown in [34], the computational complexity of **Algorithm 1** depends on the maximum CN degree, and the sizes of both the input alphabet  $\mathcal{R}$  and output alphabet  $\mathcal{A}$ . As known from (7), the maximum CN degree of the irregular LDPC code is  $d_{c,\text{max}}$ . Since we assign  $q_c$  bits to represent the output alphabet  $\mathcal{A}$ , we have  $|\mathcal{A}| \leq 2^{q_c}$ . Therefore, the complexity for calculating the alphabet  $\mathcal{A}$  is  $O(d_{c,\text{max}} \cdot 2^{q_c} |\mathcal{R}|)$ . Moreover, the DP method [36] is conducted to quantize the alphabet  $\mathcal{A}$  of size  $2^{q_c}$  into the alphabet  $\mathcal{S}$  of size  $|\mathcal{S}|$ , which has the computational complexity of  $2^{2q_c} |\mathcal{S}|$ .

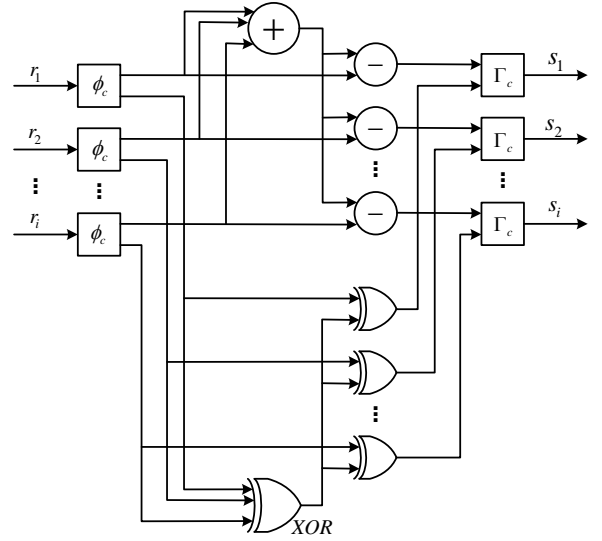


Fig. 4: Hardware architecture for the CN update of an MIM-QBP decoder.

As a result, the total computational complexity for designing the CN update is  $O(d_{c,\text{max}} \cdot 2^{q_c} |\mathcal{R}| + 2^{2q_c} |\mathcal{S}|)$  for one decoding iteration. Similarly, we use **Algorithm 2** in [34] to obtain  $\mathcal{B}$  for the VN update. According to **Algorithm 2**, the computational complexity is associated to the maximum VN degree, and the sizes of both the input alphabet  $\mathcal{S}$  and output alphabet  $\mathcal{B}$ . Since the maximum VN degree is  $d_{v,\text{max}}$  from (7) and  $\mathcal{B}$  is represented by  $q_v$  bits, the complexity for computing the alphabet  $\mathcal{B}$  is  $O(d_{v,\text{max}} 2^{q_v} |\mathcal{S}|)$ . Furthermore, to quantize the alphabet  $\mathcal{B}$  of size  $2^{q_v}$  into the alphabet  $\mathcal{R}$  of size  $|\mathcal{R}|$ , the computational complexity of the DP method is  $2^{2q_v} |\mathcal{R}|$ . Thus, the total computational complexity of designing the VN update is  $O(d_{v,\text{max}} 2^{q_v} |\mathcal{S}| + 2^{2q_v} |\mathcal{R}|)$  for one iteration.

For the design of the MIM-QMS decoder, the incoming message is mapped to the extrinsic message without the calculation and quantization for the CN update. Therefore, the computational complexity of line 6 in **Algorithm 1**, Section IV, is upper-bounded by  $2^{q_m} |\mathcal{R}|$  for the output alphabet of size  $|\mathcal{S}| = 2^{q_m}$ . With the maximum CN degree  $d_{c,\text{max}}$ , the total computational complexity is  $O(d_{c,\text{max}} \cdot 2^{q_m} |\mathcal{R}|)$  for one iteration. Since the VN update of the MIM-QMS decoder is designed in the same way as that of the MIM-QBP decoder, the computational complexity is also  $O(d_{v,\text{max}} 2^{q_v} |\mathcal{S}| + 2^{2q_v} |\mathcal{R}|)$  for one iteration.

In addition to the design complexity, the decoding complexity is another issue of great concern in practice. In the following, we start with the efficient hardware architectures to implement the node updates for the MIM-QBP decoder and then discuss the decoding complexity of the MIM quantized decoder based on the proposed architectures. Motivated by [21], the hardware architectures for the CN and VN update of the MIM-QBP decoder are presented in Fig. 4 and Fig. 5, respectively. To be more specific, Fig. 4 demonstrates the hardware architecture to compute the outgoing messages  $s_1, s_2, \dots, s_i$  for a CN with degree  $i$  ( $i \in \mathcal{D}_c$ ). The adders/subtractors and XOR gates are used for computing  $\sum_{k=1}^i |\phi_c(r_k)| - |\phi_c(r_{k'})|$  and  $(\prod_{k=1}^i \text{sgn}(\phi_c(r_k))) / \text{sgn}(\phi_c(r_{k'}))$ , respectively, where

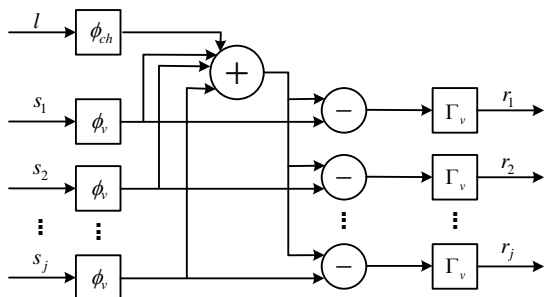


Fig. 5: Hardware architecture for the VN update of an MIM-QBP decoder.

$k' = 1, 2, \dots, i$ . Note that this architecture is applicable when  $\text{sgn}(\phi_c(\cdot)) \in \{1, -1\}$ . Moreover, Fig. 5 depicts the hardware architecture to obtain the outgoing messages  $r_1, r_2, \dots, r_j$  for a VN with degree  $j$  ( $j \in \mathcal{D}_v$ ). The adders/subtractors are utilized to calculate  $\phi_{ch}(l) + \sum_{k=1}^j |\phi_v(s_k)| - |\phi_v(s_{k'})|$  for  $k' = 1, 2, \dots, j$ .

To evaluate the decoding complexity, we denote the average CN and VN degrees by

$$\bar{d}_c = 1 / \sum_{i \in \mathcal{D}_c} \frac{\rho_i}{i} \quad \text{and} \quad \bar{d}_v = 1 / \sum_{j \in \mathcal{D}_v} \frac{\theta_j}{j}, \quad (27)$$

respectively. Based on the CN update for the MIM-QBP decoder implemented by Fig. 4, the complexity of addition and XOR operations is  $O(\bar{d}_c)$  and the complexity of table lookup operations with  $\Gamma_c$  for the  $\bar{d}_c$  outgoing messages is  $O(\bar{d}_c \lceil \log_2(|\mathcal{S}|) \rceil)$ . Hence, the average computational complexity is  $O(\bar{d}_c + \bar{d}_c \lceil \log_2(|\mathcal{S}|) \rceil)$  for one CN per iteration. Similarly, with the implementation of the VN update for the MIM-QBP decoder in Fig. 5, the computational complexity can be obtained as  $O(\bar{d}_v + \bar{d}_v \lceil \log_2(|\mathcal{R}|) \rceil)$  for one VN per iteration, where  $O(\bar{d}_v)$  refers to the complexity of addition operations, and  $O(\bar{d}_v \lceil \log_2(|\mathcal{R}|) \rceil)$  is the complexity of table lookup operations with  $\Gamma_v$  for the  $\bar{d}_v$  outgoing messages.

For the decoding of the MIM-QMS decoder, we can implement the hardware architectures such as those proposed by [37], [38], to find the first two maximum values based on (22) for the CN update while retain the hardware architecture as shown in Fig. 5 for the VN update. Consequently, the average computational complexity of searching the first two maximum values is  $O(\bar{d}_c)$  for one CN per iteration, and the computational complexity of the VN update is also  $O(\bar{d}_v + \bar{d}_v \lceil \log_2(|\mathcal{R}|) \rceil)$  for one VN per iteration. Note that the design and decoding complexity of the mapping  $Q_e$  for the bit decision of the MIM quantized decoder can be computed similarly to that of the VN update. However, we need to quantize the alphabet  $\mathcal{B}$  of size  $2^{q_v}$  into the alphabet  $\mathcal{X}$  of size  $|\mathcal{X}|$  in the design procedure and only make hard decision with  $|\Gamma_v| = 1$  for decoding. We summarize the computational complexity of the MIM quantized decoder in Table I.

## VI. SIMULATION RESULTS

In this section, we design the MIM quantized decoders with fixed precision for all iterations and evaluate the error performance of the constructed decoders via Monte-Carlo

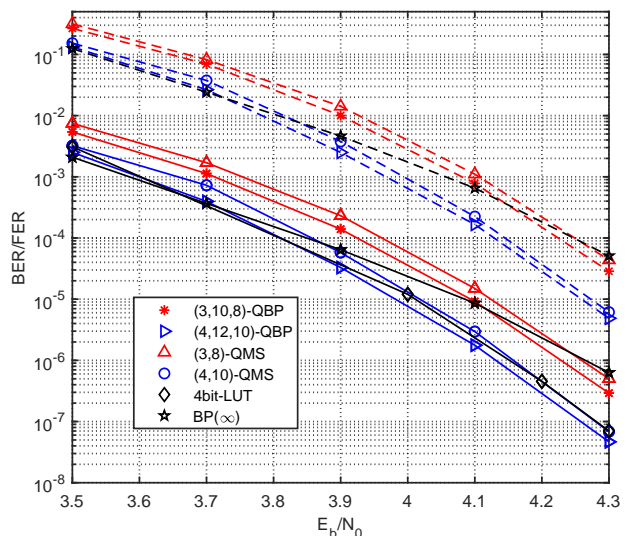


Fig. 6: BER (solid line) and FER (dash line) performance of the (6, 32) LDPC code [39] with block length 2048, code rate 0.84, and  $I_{\max} = 10$ . The BER performance of the 4bit LUT decoder is from [27, Fig. 5].

simulations. We compare the error performance of the MIM quantized decoders to that of different LUT decoder variants for both regular and irregular LDPC codes. Assume that binary LDPC codewords are modulated by binary phase-shift keying (BPSK) and randomly transmitted over the AWGNC. We denote the precision of the MIM-QBP decoder and the MIM-QMS decoder as tuple  $(q_m, q_c, q_v)$  and  $(q_m, q_v)$ , respectively. While we use notation “ $\infty$ ” to represent the floating-point precision. For convenience, we refer the MIM-QBP decoder and the MIM-QMS decoder to QBP and QMS in all figures. The operating threshold  $\sigma_d$  is also specified for each design case. In addition, at least 300 error frames are collected for each simulated SNR.

### A. The IEEE 802.3an standard LDPC Code

We first evaluate the error performance of the proposed MIM-QMS decoders for the (6, 32) regular LDPC code of block length 2048 and code rate 0.84. This code is designed for IEEE Standard 802.3an [39]. We set the maximum number of iterations  $I_{\max} = 10$ . The MIM-QMS decoders for this code are designed at  $\sigma_d = 0.5294/0.5229$  with precision (4, 10)/(3, 8), respectively. We also design the MIM-QBP decoders at  $\sigma_d = 0.5312/0.5248$  with precision (4, 12, 10)/(3, 10, 8), respectively. For comparison, we show the error performance of the LUT decoder in [27] with 4-bit message precision (i.e.,  $q_m = 4$ ), as well as that of the BP( $\infty$ ) decoder.

The bit error rate (BER) and frame error rate (FER) of different decoders are demonstrated in Fig. 6. We can see that the error performance of our proposed (4, 10) and (3, 8) MIM-QMS decoders approaches that of (4, 12, 10) and (3, 10, 8) MIM-QBP decoders within 0.05 dB, respectively. Moreover, the (4, 10) MIM-QMS decoder outperforms the BP( $\infty$ ) decoder and has nearly the same performance compared to the 4bit LUT decoder at the high SNR region. Even the (3, 8) MIM-QMS decoder achieves performance of only 0.1 dB

TABLE I: Computational Complexity per Iteration for the MIM Quantized Decoders

Mappings		Design	Decoding (per node)
$Q_c$	QBP	$O(d_{c,\max} 2^{q_c}  \mathcal{R}  + 2^{2q_c}  \mathcal{S} )$	$O(\bar{d}_c + \bar{d}_c \lceil \log_2( \mathcal{S} ) \rceil)$
	QMS	$O(d_{c,\max} 2^{q_m}  \mathcal{R} )$	$O(\bar{d}_c)$
$Q_v$		$O(d_{v,\max} 2^{q_v}  \mathcal{S}  + 2^{2q_v}  \mathcal{R} )$	$O(\bar{d}_v + \bar{d}_v \lceil \log_2( \mathcal{R} ) \rceil)$
$Q_e$		$O(d_{v,\max} 2^{q_v}  \mathcal{S}  + 2^{2q_v}  \mathcal{X} )$	$O(\bar{d}_v)$

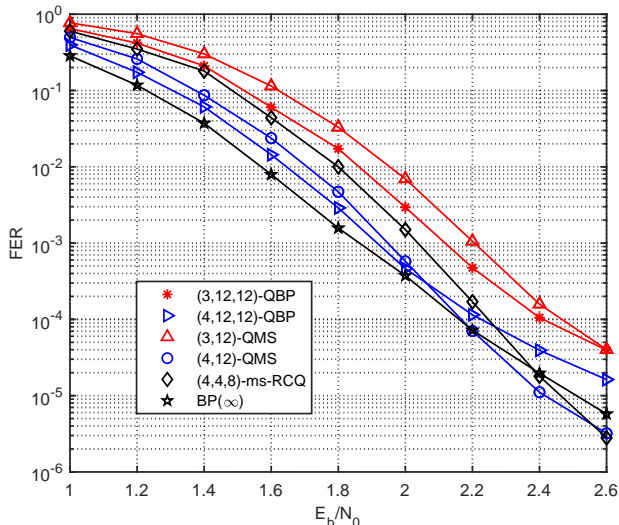


Fig. 7: FER performance of the IEEE 802.11n standard LDPC code [40] with block length 1296, code rate 0.5, and  $I_{\max} = 50$ . The FER performance of the ms-RCQ decoder is from [35, Fig. 8].

away from the  $\text{BP}(\infty)$  decoder at the low-to-moderate SNR region. While it has almost the same performance compared to the  $\text{BP}(\infty)$  decoder at the high SNR region.

### B. The IEEE 802.11n standard LDPC Code

We next investigate the FER performance of the proposed MIM-QBP decoders and MIM-QMS decoders for irregular LDPC codes. The first irregular LDPC code is selected from the IEEE 802.11n standard [40] with block length 1296 and code rate 0.5. The degree distributions of this code are given by

$$\begin{aligned} \rho(x) &= 0.8140x^6 + 0.1860x^7, \\ \theta(x) &= 0.2558x + 0.3140x^2 + 0.0465x^3 + 0.3837x^{10}. \end{aligned}$$

Here,  $I_{\max}$  is set to be 50. We build the MIM-QBP decoders at  $\sigma_d = 0.8981/0.8776$  with precision  $(4, 12, 12)/(3, 12, 12)$ , respectively. The  $(4, 12)/(3, 12)$  MIM-QMS decoders are designed at  $\sigma_d = 0.8998/0.8705$ , respectively. We also present the FER performance of the ms-RCQ decoder in [35] and the  $\text{BP}(\infty)$  decoder for comparison. Note that the precision of the ms-RCQ decoder is set as  $(4, 4, 8)$ , which is equivalent to using  $q_m = 4$  and  $q_v = 12$  for computing  $\Phi_v$  of the  $(4, 12)$  MIM-QMS decoder.

As depicted in Fig. 7, our proposed  $(4, 12, 12)$  MIM-QBP decoder and  $(3, 12, 12)$  MIM-QBP decoder have a performance degradation about 0.1 dB and 0.3 dB compared to the  $\text{BP}(\infty)$  decoder. Furthermore, the FER performance of the  $(3, 12)$  MIM-QMS decoder is about 0.4 dB away from the

$\text{BP}(\infty)$  decoder for  $\text{SNR} < 1.8$  dB. When  $\text{SNR} > 2$  dB, the  $(3, 12)$  MIM-QMS decoder approaches the FER performance of the  $\text{BP}(\infty)$  decoder within 0.3 dB. It is notable that the  $(4, 12)$  MIM-QMS decoder has a performance gain of about 0.1 dB compared to the ms-RCQ decoder and achieves the FER performance of less than 0.1 dB away from the  $\text{BP}(\infty)$  decoder when  $\text{SNR} < 2.2$  dB. When  $\text{SNR} \geq 2.2$  dB, the  $(4, 12)$  MIM-QMS decoder outperforms the  $\text{BP}(\infty)$  decoder. Note that the error floor appears for the  $\text{BP}(\infty)$  decoder and the MIM-QBP decoders. This is due to the existence of the trapping sets [26] which originates from the large amount of degree-2 VNs in the code graph. As observed in [41], the MS algorithm can overcome the trapping sets and have a better performance than the BP algorithm in the error floor region. It is shown in the figure that our proposed MIM-QMS decoder inherits this property and also surpasses the  $\text{BP}(\infty)$  decoder in terms of error floor.

### C. The Length-10000 Rate-0.5 LDPC Code

We finally evaluate the FER performance of the proposed MIM-QBP decoders and MIM-QMS decoders for the irregular LDPC code in [31] with the degree distributions specified as

$$\begin{aligned} \rho(x) &= 0.32338x^7 + 0.67662x^8, \\ \theta(x) &= 0.13805x + 0.40104x^2 + 0.02659x^8 + 0.43433x^{16}. \end{aligned}$$

This code has block length 10000 and code rate 0.5, which is optimized for the min-LUT decoder [31] with reduction of the degree-2 VNs. We set  $I_{\max} = 100$ . The operating threshold of the  $(4, 12, 12)$  MIM-QBP decoder for this code is selected as  $\sigma_d = 0.9297$ . We choose  $\sigma_d = 0.9239/0.8935$  for the MIM-QMS decoders with precision  $(4, 12)/(3, 12)$ , respectively. For comparison, we demonstrate the error performance of the 4bit LUT decoder in [27], the min-LUT decoders with the message precision of 3 and 4 bits, and the  $\text{BP}(\infty)$  decoder.

It can be seen from Fig. 8 that the  $(4, 12, 12)$  MIM-QBP decoder outperforms the 4bit LUT decoder [27] and approaches the FER performance of the  $\text{BP}(\infty)$  decoder within 0.1 dB. In addition, the proposed  $(4, 12)$  MIM-QMS decoder performs better than the 4bit min-LUT decoder [31] and has a performance gap of less than 0.05 dB from the 4bit LUT decoder. More importantly, the performance gain increases to around 0.15 dB when the  $(3, 12)$  MIM-QMS decoder is adopted compared to the 3bit min-LUT decoder. This indicates that the MIM-QMS decoder is in favor of the decoding of LDPC codes with low precision.

## VII. CONCLUSION

In this paper, we have proposed a generalized framework of the MIM quantized decoding of the LDPC codes to

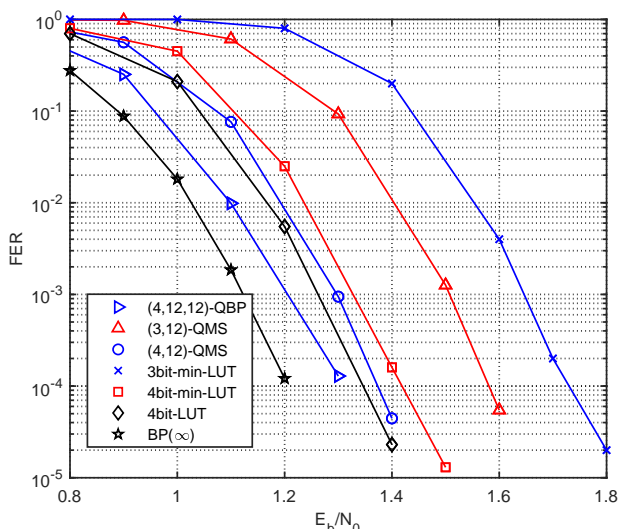


Fig. 8: FER performance of the irregular LDPC code [31] with block length 10000, code rate 0.5, and  $I_{\max} = 100$ . The FER performance of the LUT decoder and the min-LUT decoders is from [31, Fig. 12].

improve the error performance of the MIM-LUT decoding. The proposed decoding method can be designed based on either the BP or the MS algorithm, and implemented by only simple mappings and fixed-point additions. Particularly, we have proposed the max-product operation and a fast computation method for the CN update, which leads to the MIM-QMS decoder with less resource consumption and design complexity. We have also optimized the VN update by a dynamic reconstruction method, which prevents the precision degradation during the design of the decoder. For practical concerns, we discussed the choice of the channel parameter, the hardware architectures for the node updates, and the design and decoding complexity of the MIM quantized decoders. Simulation results show that the MIM-QBP decoders with 3-bit and 4-bit precision outperform the state-of-the-art LUT decoder with the same message precision at low-to-moderate SNR regions. Furthermore, the 4-bit MIM-QMS decoder has the error performance of less than 0.1 dB away from the floating-point BP decoder at low-to-moderate SNR regions and can even surpass the floating-point BP decoder at the high SNR region when decoding IEEE Standard 802.3an rate 0.84 and IEEE Standard 802.11n rate 0.5 LDPC codes.

## REFERENCES

- [1] R. G. Gallager, "Low-density parity-check codes," *IRE Trans. Inf. Theory*, vol. IT-8, no. 1, pp. 21–28, Jan. 1962.
- [2] A. J. Felstrom and K. S. Zigangirov, "Time-varying periodic convolutional codes with low-density parity-check matrix," *IEEE Trans. Inf. Theory*, vol. 45, no. 6, pp. 2181–2191, Sep. 1999.
- [3] Y. Kou, S. Lin, and M. P. C. Fossorier, "Low-density parity-check codes based on finite geometries: a rediscovery and new results," *IEEE Trans. Inf. Theory*, vol. 47, no. 7, pp. 2711–2736, Nov. 2001.
- [4] D. G. M. Mitchell, M. Lentmaier, and D. J. Costello, "Spatially coupled LDPC codes constructed from protographs," *IEEE Trans. Inf. Theory*, vol. 61, no. 9, pp. 4866–4889, Sep. 2015.
- [5] Y. Xie, L. Yang, P. Kang, and J. Yuan, "Euclidean geometry-based spatially coupled LDPC codes for storage," *IEEE J. Select. Areas Commun.*, vol. 34, no. 9, pp. 2498–2509, Sep. 2016.
- [6] M. Zhang, Z. Wang, Q. Huang, and S. Wang, "Time-invariant quasi-cyclic spatially coupled LDPC codes based on packings," *IEEE Trans. Commun.*, vol. 64, no. 12, pp. 4936–4945, Dec. 2016.

- [7] P. Chen, K. Cai, and S. Zheng, "Rate-adaptive protograph LDPC codes for multi-level-cell NAND flash memory," *IEEE Commun. Lett.*, vol. 22, no. 6, pp. 1112–1115, Jun. 2018.
- [8] T. J. Richardson and R. L. Urbanke, "The capacity of low-density parity-check codes under message-passing decoding," *IEEE Trans. Inf. Theory*, vol. 47, no. 2, pp. 599–618, Feb. 2001.
- [9] D. J. C. MacKay, "Good error-correcting codes based on very sparse matrices," *IEEE Trans. Inf. Theory*, vol. 45, no. 2, pp. 399–431, Mar. 1999.
- [10] J. Chen, A. Dholakia, E. Eleftheriou, M. P. C. Fossorier, and Xiao-Yu Hu, "Reduced-complexity decoding of LDPC codes," *IEEE Trans. Commun.*, vol. 53, no. 8, pp. 1288–1299, Aug. 2005.
- [11] V. Savin, "Self-corrected min-sum decoding of LDPC codes," in *Proc. IEEE Int. Symp. on Inf. Theory*, Jul. 2008, pp. 146–150.
- [12] T. Richardson, S. Kudekar, and L. Vincent, "Adjusted min-sum decoder," U.S. Patent 0 109 269 A1, Apr. 19, 2018.
- [13] M. P. C. Fossorier, "Iterative reliability-based decoding of low-density parity check codes," *IEEE J. Select. Areas Commun.*, vol. 19, no. 5, pp. 908–917, May. 2001.
- [14] N. Varnica, M. P. C. Fossorier, and A. Kavcic, "Augmented belief propagation decoding of low-density parity check codes," *IEEE Trans. Commun.*, vol. 55, no. 7, pp. 1308–1317, Jul. 2007.
- [15] S. Scholl, P. Schläfer, and N. Wehn, "Saturated min-sum decoding: An afterburner for LDPC decoder hardware," in *Proc. Des., Autom. and Test in Eur. Conf. Exhib.*, Mar. 2016, pp. 1219–1224.
- [16] P. Kang, Y. Xie, L. Yang, and J. Yuan, "Reliability-based windowed decoding for spatially coupled LDPC codes," *IEEE Commun. Lett.*, vol. 22, no. 7, pp. 1322–1325, Jul. 2018.
- [17] P. Kang, Y. Xie, L. Yang, C. Zheng, J. Yuan, and Y. Wei, "Enhanced quasi-maximum likelihood decoding of short LDPC codes based on saturation," in *Proc. IEEE Inf. Theory Workshop*, Aug. 2019, pp. 1–6.
- [18] T. Zhang, Z. Wang, and K. K. Parhi, "On finite precision implementation of low density parity check codes decoder," in *Proc. IEEE Int. Symp. on Circuits and Systems*, vol. 4, 2001, pp. 202–205 vol. 4.
- [19] Z. Zhang, L. Dolecek, B. Nikolic, V. Anantharam, and M. J. Wainwright, "Design of LDPC decoders for improved low error rate performance: quantization and algorithm choices," *IEEE Trans. Commun.*, vol. 57, no. 11, pp. 3258–3268, 2009.
- [20] S. Tolouei and A. H. Banihashemi, "Lowering the error floor of LDPC codes using multi-step quantization," *IEEE Commun. Lett.*, vol. 18, no. 1, pp. 86–89, 2014.
- [21] J.-S. Lee and J. Thorpe, "Memory-efficient decoding of LDPC codes," in *Proc. IEEE Int. Symp. on Inf. Theory*, Sep. 2005, pp. 459–463.
- [22] X. Zhang and P. H. Siegel, "Quantized iterative message passing decoders with low error floor for LDPC codes," *IEEE Trans. Commun.*, vol. 62, no. 1, pp. 1–14, 2014.
- [23] B. M. Kurkoski and H. Yagi, "Quantization of binary-input discrete memoryless channels," *IEEE Trans. Inf. Theory*, vol. 60, no. 8, pp. 4544–4552, Aug. 2014.
- [24] Z. Mei, K. Cai, L. Shi, and X. He, "On channel quantization for spin-torque transfer magnetic random access memory," *IEEE Trans. Commun.*, 2019.
- [25] X. He, K. Cai, W. Song, and Z. Mei, "Dynamic programming for quantization of  $q$ -ary input discrete memoryless channels," in *Proc. IEEE Int. Symp. on Inf. Theory*, Jul. 2019, pp. 450–454.
- [26] T. Richardson, "Error floor of LDPC codes," in *Proc. 41st Annu. Allerton Conf. Commun., Control, Comput.*, Monticello, IL, Oct. 2003, pp. 1426–1435.
- [27] F. J. C. Romero and B. M. Kurkoski, "LDPC decoding mappings that maximize mutual information," *IEEE J. Select. Areas Commun.*, vol. 34, no. 9, pp. 2391–2401, 2016.
- [28] J. Lewandowsky and G. Bauch, "Information-optimum LDPC decoders based on the information bottleneck method," *IEEE Access*, vol. 6, pp. 4054–4071, Jan. 2018.
- [29] M. Stark, J. Lewandowsky, and G. Bauch, "Information-optimum LDPC decoders with message alignment for irregular codes," in *Proc. IEEE Global Commun. Conf.*, Dec. 2018, pp. 1–6.
- [30] M. Stark, L. Wang, G. Bauch, and R. D. Wesel, "Decoding rate-compatible 5G-LDPC codes with coarse quantization using the information bottleneck method," *IEEE Open J. Commun. Soc.*, vol. 1, pp. 646–660, 2020.
- [31] M. Meidlinger, G. Matz, and A. Burg, "Design and decoding of irregular LDPC codes based on discrete message passing," *IEEE Trans. Commun.*, vol. 68, no. 3, pp. 1329–1343, Mar. 2020.
- [32] J. Lewandowsky, M. Stark, and G. Bauch, "Optimum message mapping LDPC decoders derived from the sum-product algorithm," in *Proc. IEEE Int. Commun. Conf.*, May 2016, pp. 1–6.

- [33] T. Cover and J. Thomas, *Elements of Information Theory*. Wiley, 2012.
- [34] X. He, K. Cai, and Z. Mei, "Mutual information-maximizing quantized belief propagation decoding of regular LDPC codes," *arXiv*, Jul. 2020. [Online]. Available: <https://arxiv.org/abs/1904.06666>
- [35] L. Wang, M. Stark, R. D. Wesel, and G. Bauch, "A reconstruction-computation-quantization (RCQ) approach to node operations in LDPC decoding," *arXiv*, May. 2020. [Online]. Available: <https://arxiv.org/abs/2005.07259>
- [36] X. He, K. Cai, W. Song, and Z. Mei, "Dynamic programming for sequential deterministic quantization of discrete memoryless channel," *arXiv*, Jan. 2019. [Online]. Available: <https://arxiv.org/abs/1901.01659>
- [37] C. Wey, M. Shieh, and S. Lin, "Algorithms of finding the first two minimum values and their hardware implementation," *IEEE Trans. Circuits Syst. I: Reg. Papers*, vol. 55, no. 11, pp. 3430–3437, Dec. 2008.
- [38] Y. Lee, B. Kim, J. Jung, and I. Park, "Low-complexity tree architecture for finding the first two minima," *IEEE Trans. Circuits Syst. II: Exp. Briefs*, vol. 62, no. 1, pp. 61–64, 2015.
- [39] *IEEE standard for information technology—telecommunications and information exchange between systems—local and metropolitan area networks-specific requirements part 3: Carrier sense multiple access with collision detection (CSMA/CD) access method and physical layer specifications*, IEEE Std. 802.3an, Sep. 2006.
- [40] *IEEE Standard for Information technology—Telecommunications and information exchange between systems—Local and metropolitan area networks-Specific requirements Part 11: Wireless LAN Medium Access Control (MAC) and Physical Layer (PHY) Specifications*, IEEE Std. 802.11n, Mar. 2012.
- [41] W. Ryan and S. Lin, *Channel codes: classical and modern*. Cambridge University Press, 2009.